

A Model System for Validation of PET Radiopharmaceuticals: Focusing on Tumor Microenvironment

Xiao-Feng Li¹, Huijie Jiang^{1,2}, Yuanyuan Ma³, Tao Huang^{1,4,5}, Xindao Yin^{1,6},
A. Cahid Civelek⁷, Baozhong Shen^{4,5}

¹Department of Diagnostic Radiology, University of Louisville School of Medicine, Louisville, USA

²Department of Radiology, The 2nd Hospital of Harbin Medical University, Harbin, China

³Memorial Sloan-Kettering Cancer Center, New York, USA

⁴Department of Radiology, The 4th Hospital of Harbin Medical University, Harbin, China

⁵Key Laboratory of Molecular Imaging, College of Heilongjiang Province, Harbin, China

⁶Imaging Center, Nanjing First Hospital Affiliated to Nanjing Medical University, Nanjing, China

⁷Department of Diagnostic Radiology, Division of Nuclear medicine, University of Louisville School of Medicine, Louisville, USA

Email: linucmed@gmail.com, shenbzh@vip.sina.com, accivelek@gmail.com

Received September 7, 2012; revised October 8, 2012; accepted October 15, 2012

ABSTRACT

Positron emission tomography (PET) imaging has emerged as an important clinical tool for cancer management, and specifically targeted radiopharmaceuticals play critical roles on PET molecular imaging. Solid cancers have highly complex and heterogeneous microenvironment, this review focused on those microenvironmental factors such as hypoxia, proliferation and perfusion and, accordingly, a novel test system for validation of current and novel targeted imaging radiopharmaceuticals. In this review, we have introduced the establishment of cancer and metastases models in nude mice, visualization of microenvironmental components of hypoxia, proliferation, perfusion, stroma and necrosis in cancers and metastases for establishing the microenvironment based model system, and validation of several radiopharmaceuticals such as ¹⁸F-fluoro-2-deoxyglucose (¹⁸F-FDG), ¹⁸F-fluorothymidine (¹⁸F-FLT), ¹⁸F-misonidazole (¹⁸F-FMISO) using the system. We found that ¹⁸F-FLT accumulates in proliferating cancer cells, while ¹⁸F-FMISO and ¹⁸F-FDG mostly accumulate in hypoxic and non-proliferative cancer cells, ¹⁸F-FDG shares roughly similar intratumoral distribution pattern with ¹⁸F-FMISO and IAZGP, but mutually excludes ¹⁸F-FLT. This model system validated current tracers for imaging glucose metabolism, hypoxia and proliferation in cancer and metastases, therefore, can be used for novel targeted radiopharmaceuticals validation.

Keywords: ¹⁸F-Fluoro-2-deoxyglucose; ¹⁸F-Fluorothymidine; ¹⁸F-Misonidazole; Microenvironment; Hypoxia; Proliferation.

1. Introduction

Positron emission tomography (PET) imaging has emerged as an important clinical tool for cancer detection, staging, and monitoring response to therapy. Current radiopharmaceuticals such as ¹⁸F-fluoro-2-deoxyglucose (¹⁸F-FDG), ¹⁸F-fluorothymidine (¹⁸F-FLT) and ¹⁸F-misonidazole (¹⁸F-FMISO) are commonly used PET tracers for cancer management. However, no tracer is conclusively superior in the management of cancer. Serial PET scans have been used in clinical studies in patients [1-7] and preclinical researches in animal models [8-14] to study the uptake mechanism of the tracers. However, the results have been mixed. This is probably due to: 1) solid cancers have highly complex and heterogeneous micro-

environment [15-17], it is impossible to generate two individual tumors with the same or similar microenvironment components and, subsequently, to compare the radiopharmaceuticals uptake in different tumors; 2) temporal change of tumor microenvironment may occur in a very short of interval of natural growth process of cancer and metastases, serial PET scans where the same tumor is probed with different tracers, separated by some time interval, are also problematic [18].

Accordingly, a novel test system is highly demand for validation of current and novel targeted radiopharmaceuticals for molecular imaging. It is established that solid cancers have highly complex and heterogeneous microenvironment [15-17] composed of viable cancer cells,

stroma, necrosis and many other factors. Viable cancer cells are either hypoxic or well oxygenated [15,16,18,19], the distribution of proliferative cells are also heterogeneous [8,10,18-21]. In this review, we focused on the discussion of hypoxia, proliferation and perfusion microenvironment factors of cancer and metastases in animal model and its usefulness in PET tracers validation. We initially introduced the generation of cancer and metastases models in nude mice, then characterization of hypoxia, proliferation, perfusion, stroma and necrosis in cancer and metastasis using histological/immunohistochemical techniques, and finally, the relationship of radiopharmaceuticals accumulation and microenvironmental factors [18].

2. Animal Models of Cancers and Metastases

Models of disseminated microscopic malignant disease may be generated in the lung, bone, liver and peritoneum by intravenous [22-24], left ventricular [22,25], intrasplenic [26] and intraperitoneal [8,18,19,27,28] injection of tumor cells, respectively. We have shown that a model of disseminated microscopic peritoneal and ascites tumors was suitable for studying hypoxia [8,18,19,27,28]. In this model, disseminated peritoneal microscopic tumors were induced by injecting suspensions of colorectal HT29 and HCT-8 cancer cells, or non-small cell lung cancer (NSCLC) A549 and HTB177 cells into the peritoneal cavity of nude mice. Mice sacrificed 4 - 7 weeks after tumor initiation displayed a distribution of tumors of sizes ranging from a few hundred micrometers up to several millimeters in diameter on or in the intestinal serosa (**Figure 1**). Ascites fluid containing a distribution of free-floating tumor cell aggregates of up to 1 mm in diameter was also present in mice inoculated with HT29, A549 cells, but was not observed in HCT-8 and HTB177 cell lines.



Figure 1. HCT-8 rectal cancer cells peritoneal metastases formed 4 wk after intraperitoneal administration of cancer cells, tumors ranged from several hundred micrometers to millimeters in diameter.

Intradermal injection of similar tumor cell suspensions could give rise to unitary microscopic tumors useful for studying hypoxia [8,19,27]. An intradermal tumor model has the potential advantage that growth curves for microscopic tumors could be more easily generated via ultrasound or optical imaging. Subcutaneous xenografts generated by subcutaneously injection of cancer cells are widely used for microPET study.

3. Tumor Microenvironment

3.1. Visualization of Hypoxia, Proliferation, Perfusion and Vasculature

Hypoxia microenvironment visualization relies on the detection of either exogenous substances (tracers) that preferentially localizes in hypoxic tissue or the expression of hypoxia-induced endogenous markers [28]. The most commonly used exogenous hypoxia markers, including pimonidazole, EF5 and CCI-103F, are 2-nitroimidazole compounds that are selectively reduced in hypoxic regions (generally $pO_2 < 10$ mmHg) of tumors, subsequently binding to intracellular macromolecules [28, 29]. The spatial pattern of binding of these markers can be visualized on tumor sections by immunohistochemical methods. Exogenous hypoxia markers have been widely used in clinical and experimental studies of tumor hypoxia [30-33]. Pimonidazole is used to visualize tumor hypoxia in our group, which is generally administrated 1-2 hours before animal sacrifice.

A large number of cellular proteins are regulated by hypoxia. Potential endogenous markers of hypoxia include hypoxia inducible factor 1 α (HIF1 α), carbonic anhydrase 9 (CA9) [19] and glucose transporters 1 (GLUT1) [8,28]. The degradation of CA9 is a relatively slow process with estimated half-times of a few days [19] which would more appropriately indicate “historical” hypoxia. Thus combinations of endogenous protein markers used in conjunction with exogenous tracers can be used to detect changes in tumor hypoxia. Such an approach may be used to monitor the effect of interventions that perturb the intratumoral distribution of hypoxia [8,19].

The cellular proliferation marker bromodeoxyuridine was administered via tail vein injection 1hr before animal sacrifice to detect proliferative cancer cells [8,18,19]. Vasculature was visualized by Anti-CD31 staining [19,28]. Perfusion was detected by fluorescent dye Hoechst 33342 which was administered via tail vein injection 1 minute before animal sacrifice [19]. Hematoxylin and eosin (H&E) provided information of viable cancer cells, stroma and necrosis with the tumor section.

3.2. Hypoxia, Proliferation, Perfusion in Microscopic Tumors

Disseminated peritoneal disease developed after intrape-

ritoneal inoculation of tumor cells. At the time of assay the gross appearance of peritoneal disease was similar for both cell lines, consisting of a distribution of small tumors adhering to the intestinal serosa [8,19,28]. Tumor sizes ranged from a few hundred μm to several mm in diameter. Microscopic examination of peritoneal tumor sections indicated a characteristic relationship between the pattern of hypoxia and tumor size. In general, sub-millimeter tumor deposits (<1 mm diameter) showed intense pimonidazole staining coupled with low Hoechst 33342 staining (**Figure 2(a)**). This observation was indicative of hypoxic and relatively poorly perfused tumors. Larger tumors ($\sim 1 - 4$ mm diameter) appeared relatively well perfused with generally low levels of pimonidazole staining. Anti-CD31 staining (**Figure 2a**) showed a contrast in tumor vascularity between the tumors of different size with the smallest tumors possessing little to no vasculature while larger tumors were well-vascularized. bromodeoxyuridine staining indicated that cellular proliferation tended to occur in the rim but not the interior of small avascular tumors (**Figure 2(b)**) whereas it was prevalent throughout larger tumors [8,19,28].

3.3. Hypoxia, Proliferation, Perfusion in Microscopic Intradermal Tumors

The patterns of hypoxia in intradermal tumors, ranging from a few hundred μm to several millimeters in diameter, were examined. Smaller intradermal tumors (<1 mm in diameter) were characterized by a high level of pimonidazole positivity and little to no visible Hoechst 33342 or CD31 positivity (**Figure 2(c)**). In HT29 tumors, positive CA9 staining co-localized with pimonidazole. It was also observed that small intradermal tumors generally contained significant central necrosis. In contrast, for larger intradermal tumors ($\sim 1 - 4$ mm in diameter) pimonidazole staining appeared less intense, Hoechst 33342 was present throughout, together with significant vascularity and minimal necrosis (**Figure 2(c)**) [19,28].

3.4. Hypoxia and Perfusion in Ascites Tumors

On microscopic examination HT29 ascites tumors appeared similar to small avascular HT29 peritoneal tumors of <1 mm in diameter (**Figure 2(d)**). Ascites tumors stained intensely positive for pimonidazole and CA9 but negative for Hoechst 33342, indicating that they were mostly hypoxic with little to no blood perfusion [8,19,27].

3.5. Microenvironment of Macroscopic Subcutaneous Tumors

Macroscopic subcutaneous tumors have intermingled but clearly defined regions of non-cancer cell stroma, cancer cells and necrosis. **Figure 3(a)** shows an example of complex microenvironment revealed by H&E imaging

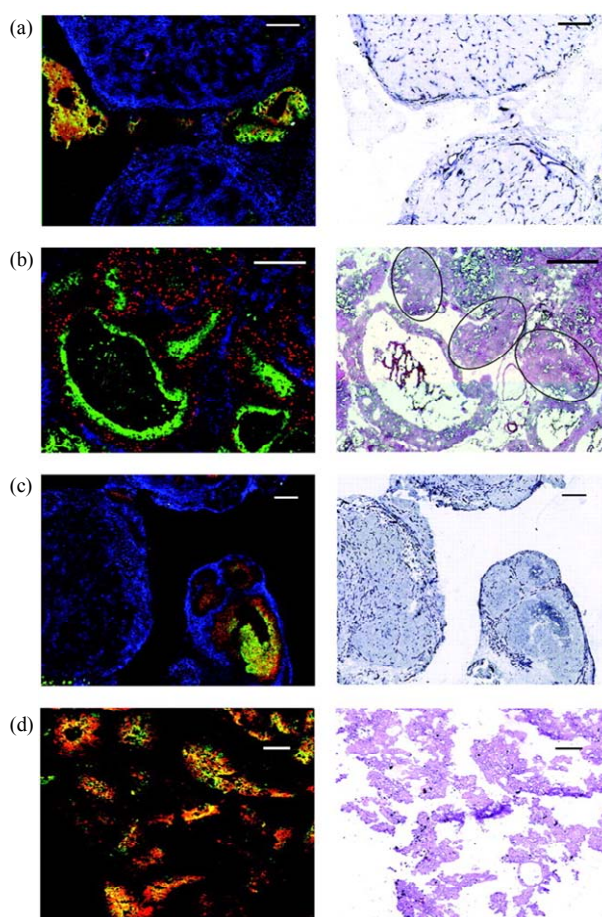


Figure 2. Representative images of microscopic HT29 tumors. (a) Left: Fluorescence overlay image (green = pimonidazole, blue = Hoechst 33342, red = CA9) of a section containing a variety of large and small peritoneal tumors. The series of small tumors $\leq 500 \mu\text{m}$ in dimension situated along a horizontal line through the center of the figure all show intense pimonidazole and CA9 fluorescence, suggesting significant hypoxia, with little to no Hoechst 33342 fluorescence. This contrasts with the two large tumor deposits that extend towards the top and bottom of the image which show extensive Hoechst 33342 but little pimonidazole or CA9 fluorescence. Scale bar, $200 \mu\text{m}$. (a) Right: Contiguous section stained for CD31. It can be seen that the small tumors that appear hypoxic in (a) left are essentially avascular whereas the large tumors have extensive vasculature. (b) Left: fluorescence overlay image (green = pimonidazole, blue = Hoechst 33342, red = bromodeoxyuridine) of a section containing a mixture of small peritoneal tumors of various sizes together with stromal components. Three small deposits with dimensions of approximately $300 \mu\text{m}$ (indicated on (b) right) all show intense central pimonidazole fluorescence with little to no Hoechst 33342 implying significant hypoxia and low perfusion. Bromodeoxyuridine (red) fluorescence indicating cellular proliferation is seen only in the non-hypoxic rim and is not present in the hypoxic core. Scale bar, $200 \mu\text{m}$; (b) Right: Contiguous section stained with hematoxylin and eosin provided for reference. (c) Left: Fluorescence overlay image (green = pimonidazole, blue = Hoechst 33342, red = CA9) of a section containing two intradermal

tumors. The smaller tumor (right) consists of three distinct nodules, each centrally-hypoxic with varying necrosis, separated by highly perfused zones. The larger tumor (left) appears minimally hypoxic with widespread perfusion throughout. Scale bar, 200 μm ; (c) Right: Contiguous section stained for CD31. The hypoxic tumor nodules appear essentially avascular while there is significant vascularity seen in the well-perfused stromal elements, between nodules. The larger non-hypoxic tumor has extensive vasculature. (d) Left: fluorescence overlay image (green = pimonidazole, red = CA9) of a section containing a collection of HT29 ascites tumors. Widespread intense staining is observed for both pimonidazole and CA9 implying significant hypoxia. Scale bar, 400 μm ; (d) Right: Contiguous section stained with hematoxylin and eosin provided for reference. Figure 2 is adapted from [19].

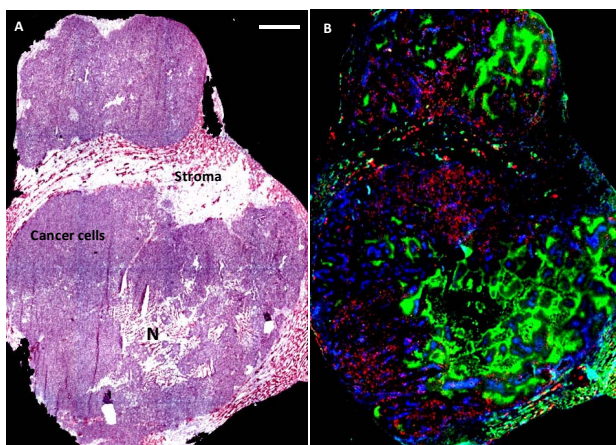


Figure 3. Complex microenvironment of HTB177 subcutaneous xenograft. (a) H&E: the xenograft is composed with stroma, cancer cells and necrosis (N). Scale bar = 1 mm; (b) Fluorescence overlay image of a contiguous section to H&E stained section shows hypoxia, proliferation and blood perfusion of cancer cells. pimonidazole (green); Hoechst 33342 (blue); bromodeoxyuridine (red). All Scale bars = 1 mm. This research was originally published in *JNM*. T. Huang, A. C. Civelek, J. Li, H. Jiang, C. K. Ng, G. C. Postel, B. Shen and X. F. Li, "Tumor Microenvironment-Dependent 18F-FDG, 18F-Fluorothymidine, and 18F-Misonidazole Uptake: A Pilot Study in Mouse Models of Human Non-Small Cell Lung Cancer," *Journal of Nuclear Medicine*, Vol. 53, 2012, pp. 1262-1268 © by the Society of Nuclear Medicine, Inc.

from NSCLC HTB177 subcutaneous xenograft. Cancer cells were further divided into two subcategories according to oxygenation status and cellular proliferation (**Figure 3(b)**): cancer cells closely adjacent to functional blood vessels (positive Hoechst 33342 staining) were stained negative for pimonidazole but positive for bromodeoxyuridine, indicating well oxygenated and highly proliferative. Cancer cells located approximately 150 μm away from functional blood vessels and/or close to necrosis were stained positive for pimonidazole but negative for bromodeoxyuridine, which indicated that these cancer cells were hypoxic with low proliferation rate [18].

Apparently, macroscopic solid cancers have complex microenvironment.

3.6. Relationship between Hypoxia and Tumor Size

The pimonidazole positive fraction (PPF) was estimated for a range of non-ascites HT29 tumors of various sizes (**Figure 4**) [19]. This reveals an interesting size-dependency of tumor hypoxia. For the smallest peritoneal and intradermal tumors PPF was very high, approaching $\sim 90\%$ in tumors of several hundred μm diameter. At these sizes, tumors were relatively avascular. As peritoneal and intradermal tumors increased in size, the PPF decreased until in the range of diameters $\sim 1 - 4$ mm there was little to no positive pimonidazole staining, indicating little to no tumor hypoxia, coupled with the appearance of tumor vascularization and significant blood perfusion. As tumor size increased further into the diameter range ≥ 4 mm, positive pimonidazole staining reappeared in a characteristically perinecrotic distribution pattern that was inversely correlated with Hoechst 33342-defined perfusion.

We have visualized hypoxia, proliferation and perfusion in cancer and metastases models. The microenvironment-based model system has been used to validate and test several current PET tracers for imaging glucose metabolism, hypoxia and proliferation by our group [8,18,27].

4. Examine Radiopharmaceuticals Using the Characterized Model System

Such model system may provide a useful means of corroborating the validity of purported targeted tracers. There are powerful methods of assessing the microenvi-

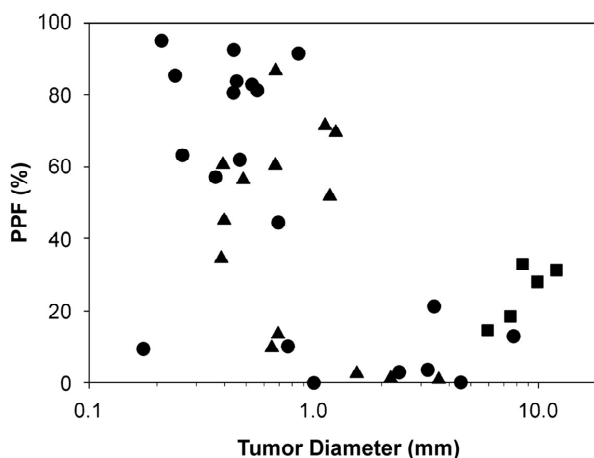


Figure 4. Scatterplot showing the relationship between tumor size and Pimonidazole positive fraction (PPF) for HT29 tumors. ● Peritoneal; ▲ Intradermal; ■ Subcutaneous. Adapted from [19].

ronmental features of individual microscopic tumors, including their hypoxic status, proliferation and blood perfusion, and relating these to the uptake of radiolabeled tracer. In addition, such models provide a diversity of tumors of differing size and hypoxic status growing in the same animal, thereby reducing or eliminating issues associated with inter-animal variability. To complement the high spatial resolution associated with immunohistochemical detection of hypoxia markers, the intratumoral distribution of radiolabeled hypoxia tracers can be determined by DAR detection systems. Studies comparing the spatial distributions of radiolabeled tracers and hypoxia markers have been reported in macroscopic tumors [10,18,34] and microscopic diseases [8,18,27].

4.1. ^{18}F -FDG

^{18}F -FDG PET has emerged as an important clinical tool for cancer detection, staging, and monitoring of response and is routinely used in the clinical management of several cancer types [35]. The uptake of ^{18}F -FDG, an analog of glucose, is largely proportional to the rate of glucose metabolism enabling this parameter to be quantified [36]. In hypoxic conditions, cancer cells may undergo a switch from aerobic to anaerobic glucose metabolism. This adaptive response involves the coordinated expression of many hypoxia inducible factor (HIF)-regulated proteins, such as GLUT-1, and various glycolytic enzymes [37]. Glucose metabolism in hypoxic cancer cells has been studied in cell culture and in animal models of macroscopic tumors (reviewed in [36]), however, results have been mixed and controversial.

We have recently reported the use of correlative imaging methodologies to examine the uptake of ^{18}F -FDG in microscopic [8] and macroscopic [18] tumors and relate this to hypoxic status. ^{18}F -FDG uptake by DAR was compared with immunofluorescent visualization of pimonidazole binding and GLUT-1 expression. We have also reported that ^{18}F -FDG uptake in microscopic tumors was altered by carbogen breathing [8].

^{18}F -FDG uptake in disseminated peritoneal disease arising from HT29, HCT-8, A549 and HTB177 tumor cells was studied in air-breathing animals [8,18]. As shown in **Figure 5**, there was spatial co-localization between high levels of ^{18}F -FDG uptake, pimonidazole binding and GLUT-1 expression. Such regions tended to correspond to low levels of cellular proliferation and blood perfusion. In particular, the smallest tumor deposits (<~1 mm diameter) were hypoxic (as evidenced by high pimonidazole binding) and had high ^{18}F -FDG uptake. In these tumors GLUT-1 expression was high, bromodeoxyuridine staining was confined to the rim and blood perfusion was minimal. Larger tumors (~1 - 4 mm diameter) were not hypoxic (low pimonidazole binding) and displayed relatively low ^{18}F -FDG uptake and GLUT-

1 expression. Additionally, bromodeoxyuridine-positive proliferative cells were distributed throughout the larger tumors and blood perfusion was relatively high.

Carbogen breathing significantly decreased ^{18}F -FDG accumulation and tumor hypoxia in microscopic tumors but had little effect on GLUT1 expression (**Figure 6**) [8].

^{18}F -FDG uptake in subcutaneous xenografts was also observed. High ^{18}F -FDG uptake was found in hypoxic zones but low ^{18}F -FDG uptake in well perfused cancer cells, non-cancerous stroma and necrosis (**Figure 7**) [18].

Therefore, ^{18}F -FDG uptake was significantly increased in microscopic tumors and only hypoxic regions of macroscopic tumors. This enhanced uptake could be abrogated by carbogen breathing; physiological hypoxia was a necessary condition for increased ^{18}F -FDG uptake.

4.2. Radioiodine-Labeled-Iodoazomycin Galactopyranoside and ^{18}F -FMISO

Radiolabeled tracers such as ^{18}F -FMISO [38-40] and ^{124}I -labelled iodo-azomycin galactopyranoside (^{124}I -IAZGP) [41-43], amongst others are under investigation for *in vivo* PET imaging of tumor hypoxia. We have recently reported the use of correlative imaging methodologies to examine the uptake of IAZGP and ^{18}F -FMISO in microscopic [18,27] and macroscopic [18] tumors and related this to microenvironmental factors.

Figure 8 shows an example of the intratumoral distributions of ^{131}I -IAZGP, pimonidazole binding and CA9

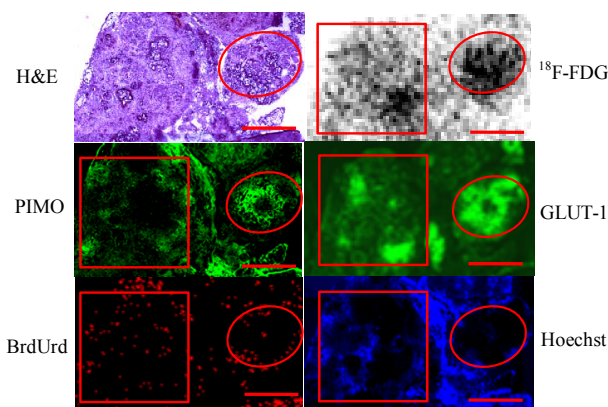


Figure 5. ^{18}F -FDG uptake in HT29 peritoneal tumors in air breathing condition. Part of a larger tumor (square) has relatively low levels of ^{18}F -FDG uptake, pimonidazole binding, and GLUT-1 expression, with relatively high levels of cell proliferation and blood perfusion. A microscopic tumor (circle) has relatively high FDG uptake, pimonidazole binding and GLUT-1 with lower cell proliferation and little perfusion. Scale bar 1 mm. This research was originally published in *JNM*. X. F. Li, Y. Ma, X. Sun, J. L. Humm, C. C. Ling and J. A. O'Donoghue, "High ^{18}F -FDG Uptake in Microscopic Peritoneal Tumors Requires Physiologic Hypoxia," *Journal of Nuclear Medicine*, Vol. 5, 2010, pp. 632-638 © by the Society of Nuclear Medicine, Inc.

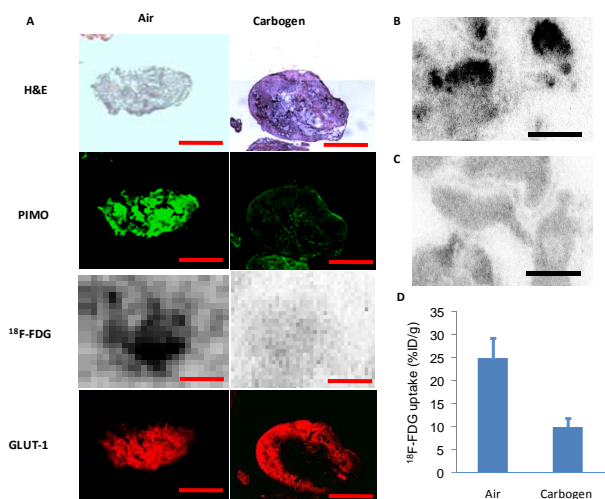


Figure 6. (a) Comparison of HT29 peritoneal tumors from animals breathing air or carbogen (95% O₂, 5% CO₂). ¹⁸F-FDG uptake and pimonidazole binding were markedly reduced for carbogen breathing whereas GLUT-1 expression was unaffected (see text for details). Scale bar 500 μm; (b) For air breathing conditions, overall ¹⁸F-FDG uptake was higher and a number of “hot spots” were observed. In contrast, carbogen breathing; (c) Resulted in significantly less ¹⁸F-FDG uptake in microscopic tumors, scale bars 4 mm; (d) The difference in ¹⁸F-FDG uptake between sub-millimeter HT29 tumors in air-breathing (9 tumors from 2 animals) and carbogenbreathing (11 tumors from 2 animals) animals was significant, *p* < 0.001. *JNM*, Vol. 5, 2010, pp. 632-638 © by the Society of Nuclear Medicine, Inc.

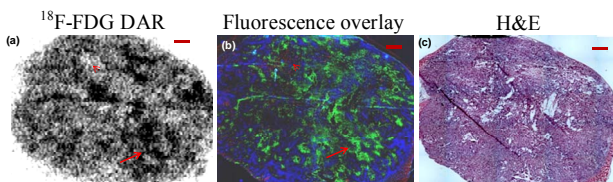


Figure 7. Relationship between ¹⁸F-FDG uptake and hypoxia, proliferation and blood perfusion in a HTB177 subcutaneous xenograft. High ¹⁸F-FDG uptake (a) detected by digital autoradiography (DAR) is found in hypoxic (pimonidazole positive, green) but lowly proliferating (bromodeoxyuridine negative, red) cancer cells (b) (arrow). Non-hypoxic and proliferative cancer cells (bromodeoxyuridine positive, red) which are well blood perfused (Hoechst positive, blue), have low ¹⁸F-FDG uptake (arrow head). Stroma and necrotic zones associate with low ¹⁸F-FDG activity. H&E from adjacent section provided for reference (c). All scale bars =1 mm. This research was originally published in *JNM*. T. Huang, A. C. Civelek, J. Li, H. Jiang, C. K. Ng, G. C. Postel, B. Shen and X. F. Li, “Tumor Microenvironment-Dependent 18F-FDG, 18F-Fluorothymidine, and 18F-Misonidazole Uptake: A Pilot Study in Mouse Models of Human Non-Small Cell Lung Cancer,” *JNM*, Vol. 53, 2012, pp. 1262- 1268 © by the Society of Nuclear Medicine, Inc.

expression in a small (~1 mm dimension) and relatively large tumor obtained from an animal with disseminated colorectal cancer HT29 peritoneal disease [27]: the smaller

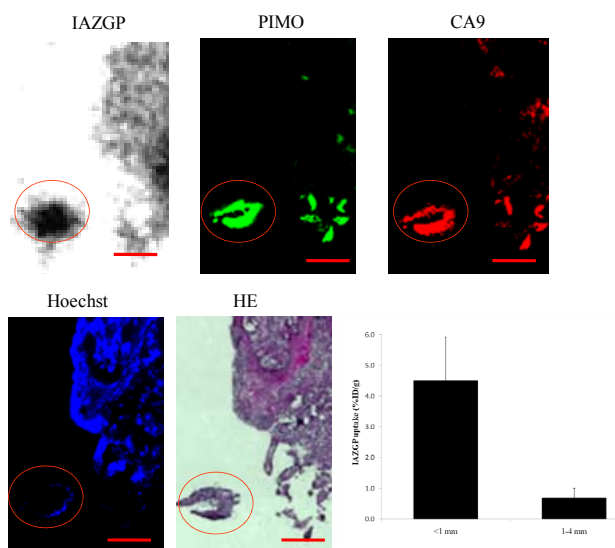


Figure 8. Comparison of intratumoral distribution of ¹³¹I-IAZGP with pimonidazole binding (green), hypoxia-regulated protein CA9 (red) and Hoechst 33342 (blue) in a tissue section containing disseminated intraperitoneal (i.p.) HT29 tumors. A larger tumor, part of which is seen in the upper right quadrant has low levels of ¹³¹I-IAZGP uptake, pimonidazole binding and CA9 expression together with significant blood perfusion. The microscopic tumor with dimensions of ~1 mm (circled) has high ¹³¹I-IAZGP uptake throughout the tumor together with high pimonidazole binding and CA9 expression. All images were obtained from the same tissue section. Scale bar =1 mm. The histogram shows quantitative ¹³¹I-IAZGP uptake in a collection of 27 i.p. HT29 tumors from a single animal expressed as % injected dose per gram. Tumor uptake was derived from an ¹³¹I-IAZGP autoradiograph with individual tumor sizes based on the H&E image. ¹³¹I-IAZGP uptake was significantly higher in microscopic i.p. tumors (<1 mm diameter, *n* = 18) than larger ones (>1 mm, *n* = 9), *p* < 0.001. Adapted from [27].

tumor shows elevated uptake of ¹³¹I-IAZGP and near-ubiquitous staining of pimonidazole and CA9, implying almost uniform hypoxia. The larger tumor shows reduced ¹³¹I-IAZGP uptake and low levels of pimonidazole binding and CA9 expression together with significant Hoechst 33342 uptake indicating that the tumor was well-perfused.

Microscopic ascites tumors had high ¹³¹I-IAZGP uptake coupled with intense staining of pimonidazole and CA9 (Figure 9) [27]. ¹³¹I-IAZGP uptake was also tested in intradermal tumors [27]. The smaller tumor (<1 mm in diameter) was characterized by a central lack of blood perfusion, high levels of co-localized pimonidazole binding and CA9 expression and high ¹³¹I-IAZGP accumulation. In contrast, intradermal tumors above 1 mm in diameter were well perfused, had low ¹³¹I-IAZGP and pimonidazole accumulation and had low CA9 expression (Figure 10).

Intratumoral distribution of ¹⁸F-FMISO was observed

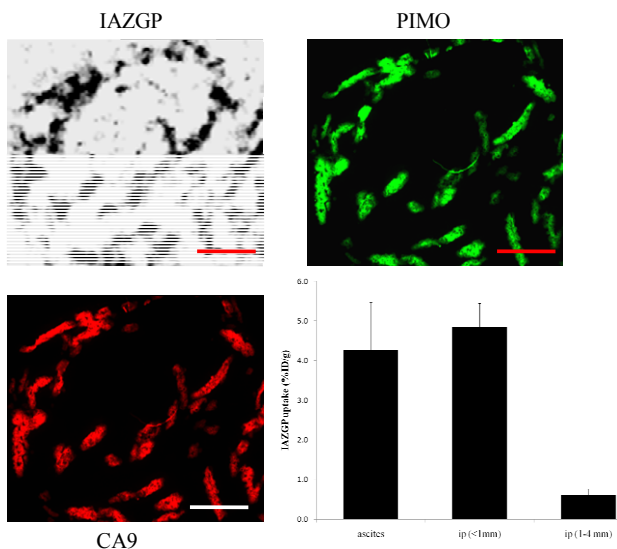


Figure 9. High levels of ¹³¹I-IAZGP uptake pimonidazole binding and CA9 expression in HT29 ascites tumors from a single animal. Scale bar = 1 mm. The histogram shows quantitative ¹³¹I-IAZGP uptake in a collection of 13 ascites and intraperitoneal (i.p.) tumors from a single animal. Uptake in ascites and smaller i.p. tumors was significantly higher than in larger tumors, *p* < 0.001. Adapted from [27].

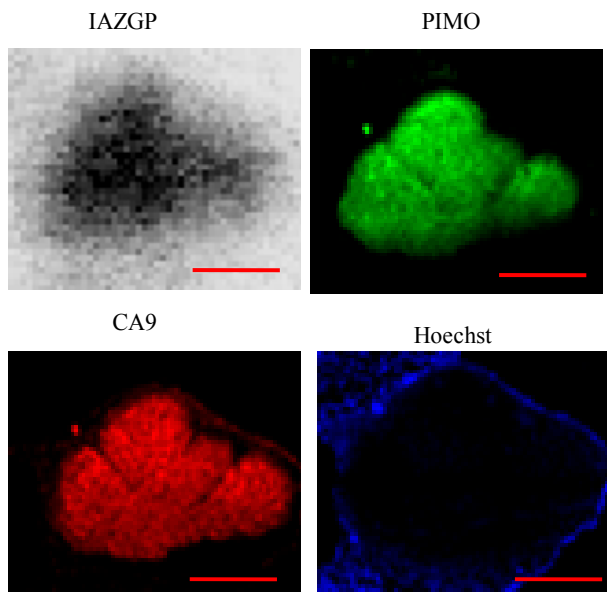


Figure 10. Comparison of intratumoral distribution of ¹³¹I-IAZGP uptake, pimonidazole binding, CA9 expression and blood perfusion in a microscopic HT29 intradermal (i.d.) tumor. The microscopic tumor shows high ¹³¹I-IAZGP uptake, pimonidazole binding and CA9 expression with little to no blood perfusion. Scale bar = 500 μm. Adapted from [27].

in subcutaneous xenografts and peritoneal tumors of NSCLC. High levels of ¹⁸F-FMISO uptake and pimonidazole binding were colocalized [18]. Such regions tended to correspond to low levels of cellular proliferation

and blood perfusion. Well oxygenated cancer cells with a high proliferation rate had low ¹⁸F-FMISO uptake. Stroma and necrotic zones had lower ¹⁸F-FMISO accumulation (**Figure 11**) [18].

We have validated that ¹³¹I-IAZGP and ¹⁸F-FMISO as hypoxia imaging tracers in colorectal and NSCLC microscopic and macroscopic tumor models, in which tumor microenvironment was characterized by immunohistochemical staining. Therefore, this model system is useful for validating current and novel hypoxia-imaging tracers.

4.3. ¹⁸F-FLT

¹⁸F-FLT PET has been used to assess proliferation in cancer. We have used ¹⁸F-FLT to test our model system [18]. ¹⁸F-FLT preferentially accumulated in areas of tumor that showed high uptake of bromodeoxyuridine and low staining of pimonidazole. This was demonstrated for NSCLC cell lines A549 and HTB177, grown as either subcutaneous xenografts or disseminated peritoneal disease. For example, in HTB177 peritoneal tumors (**Figure 12**), high ¹⁸F-FLT uptake was found in the regions with high levels of bromodeoxyuridine binding (proliferative) cancer cells where pimonidazole stained negatively indicating well oxygenated. Low ¹⁸F-FLT accumulation was found in cancer cells which were stained positive for pimonidazole (hypoxia) but low for bromodeoxyuridine (low proliferation). Stroma and necrotic zones also associated with low ¹⁸F-FLT accumulation. ¹⁸F-FLT uptake significantly correlated with proliferation index (*r* = 0.91, *p* < 0.001) [18]. Therefore, our model system enables to validate current and novel tracers imaging proliferation.

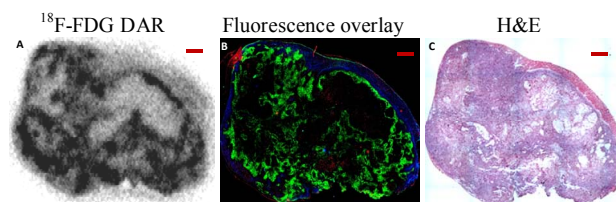


Figure 11. Relationship between ¹⁸F-FMISO uptake and hypoxia, proliferation and blood perfusion in an A549 subcutaneous xenograft. High ¹⁸F-FMISO uptake (a) closely associates with hypoxic (pimonidazole positive, green, (b)) cancer cells. Non-hypoxic cancer cells are proliferative (bromodeoxyuridine positive, red) and well blood perfused (Hoechst positive, blue), have low ¹⁸F-FMISO uptake. Stroma and necrotic zones associate with low ¹⁸F-FMISO activity. H&E from adjacent section provided for reference (c). All scale bars = 1 mm. This research was originally published in *JNM*. T. Huang, A. C. Civelek, J. Li, H. Jiang, C. K. Ng, G. C. Postel, B. Shen and X. F. Li, “Tumor Microenvironment-Dependent ¹⁸F-FDG, ¹⁸F-Fluorothymidine, and ¹⁸F-Misonidazole Uptake: A Pilot Study in Mouse Models of Human Non-Small Cell Lung Cancer,” Vol. 53, 2012, pp. 1262-1268 © by the Society of Nuclear Medicine, Inc.

5. The Importance of Animal Models of Metastases for Novel Targeted Radiopharmaceuticals Development

Animal models of metastases as a test system for radiotracer validation have several advantages compared with macroscopic subcutaneous xenografts. Individual small tumors have an approximately homogenous internal structure, being either hypoxic and unperfused, or non-hypoxic and well perfused. This makes it relatively simple to demonstrate co-localization of radiotracer and hypoxia marker (immunofluorescence). In contrast, macroscopic xenografts have a complex internal structure with intermingled regions of non-cancerous stroma, well oxygenated tumor, hypoxia and necrosis in close proximity. Another advantage is that since many tumors of various sizes and degrees of hypoxia can exist in an individual animal, it is possible to compare radiotracer uptake between tumors without confounding variations due to dif-

ferences in injected dose or inter-animal pharmacokinetics [8,18,27]. Therefore, metastatic model is a valuable supplement to macroscopic xenograft models as a test system for novel molecular imaging tracer development. It should be emphasized here that macroscopic xenograft model is still very important in PET studies.

There are some limitations for using autoradiograph and immunohistochemical staining techniques to study tumor hypoxia. Hypoxia can be chronic (perfusion limited) hypoxia or acute hypoxia (transient hypoxia, or diffusion-limited"). To some extent, immunohistochemical staining of hypoxia marker seems to be unable to distinguish chronic hypoxia from acute hypoxia, therefore a general term "hypoxia" is used throughout the article; Transient hypoxia is observed to be an important factor for radiotherapy resistance and is difficult to figure out, Wang and colleagues have recently established a model to successfully identify hypoxia with dynamic PET scan [44].

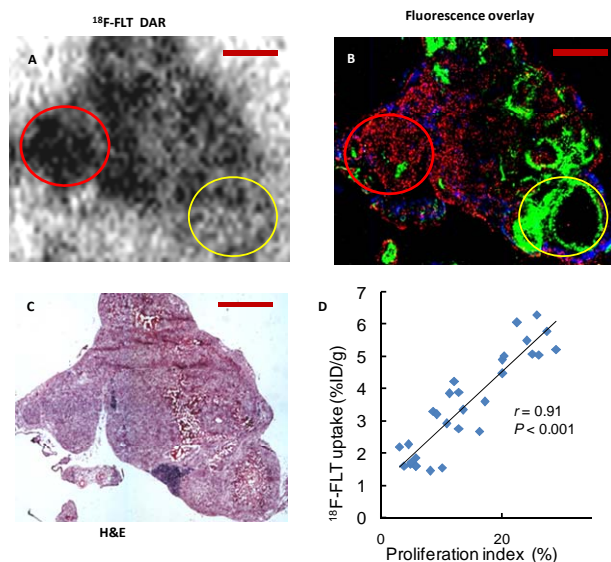


Figure 12. Relationship between ^{18}F -FLT uptake and hypoxia, proliferation and blood perfusion in HTB177 peritoneal tumor model. High ^{18}F -FLT accumulation (a) is found in highly proliferating cancer cells (bromodeoxyuridine positive, red) which are not hypoxia (pimonidazole negative) and well blood perfused (Hoechst positive, blue) (red circle) (b). Pimonidazole positive (green) cancer cells have little ^{18}F -FLT uptake (yellow circle). Stroma and necrotic zones associate with low ^{18}F -FLT activity. H&E from adjacent section provided for reference (c). Correlation between bromodeoxyuridine defined proliferative index and ^{18}F -FLT, $r = 0.91$, $p < 0.001$ (d). All scale bars =1 mm. This research was originally published in *JNM*. T. Huang, A. C. Civelek, J. Li, H. Jiang, C. K. Ng, G. C. Postel, B. Shen and X. F. Li, "Tumor Microenvironment-Dependent ^{18}F -FDG, ^{18}F -Fluorothymidine, and ^{18}F -Misonidazole Uptake: a Pilot Study in Mouse Models of Human Non-Small Cell Lung Cancer," *Journal of Nuclear Medicine*, Vol. 53, 2012, pp. 1262-1268 © by the Society of Nuclear Medicine, Inc.

6. Conclusion

This review has introduced the establishment of cancer and metastases models and characterization of tumor microenvironment including hypoxia, proliferation, perfusion, stroma in the experimental tumors. The microenvironment-based model system enables to validate several radiopharmaceuticals such as ^{18}F -FDG, ^{18}F -FLT and ^{18}F -FMISO and IAZGP. ^{18}F -FLT accumulates in proliferating cancer cells, while as ^{18}F -FMISO, IAZGP and ^{18}F -FDG mostly accumulate in hypoxic and non-proliferative cancer cells, ^{18}F -FDG shares roughly similar intratumoral distribution pattern with ^{18}F -FMISO and IAZGP, but mutually excludes ^{18}F -FLT. This model system would be useful for validating current and, therefore, novel tracers imaging glucose metabolism, hypoxia, proliferation and possibly others.

7. Acknowledgments

We thank Mr. Dylan T. Lovan at The Associated Press to edit the manuscript. The authors' current work is supporting by Kentucky Lung Cancer Research Program, National Natural Science Foundation of China (81130028) and Science and Technique Foundation of Heilongjiang Province (major program, GA12C302). The authors have no conflict of interest relevant to this article.

REFERENCES

- [1] T. Zander, M. Scheffler, L. Nogova, C. Kobe, W. Engel-Riedel, M. Hellmich, I. Papachristou, K. Toepelt, A. Draube, L. Heukamp, R. Buettner, Y. D. Ko, R. T. Ul-lich, E. Smit, R. Boellaard, A. A. Lammertsma, M. Hallek, A. H. Jacobs, A. Schlesinger, K. Schulte, S. Querings, E. Stoelben, B. Neumaier, R. K. Thomas, M. Dietlein and

- J. Wolf, "Early Prediction of Nonprogression in Advanced Non-Small-Cell Lung Cancer Treated with Erlotinib by Using [^{18}F] Fluorodeoxyglucose and [^{18}F]Fluorothymidine Positron Emission Tomography," *Journal of Clinical Oncology*, Vol. 29, No. 13, 2011, pp. 1701-1708. [doi:10.1200/JCO.2010.32.4939](https://doi.org/10.1200/JCO.2010.32.4939)
- [2] V. Frings, A. J. de Langen, E. F. Smit, F. H. van Velden, O. S. Hoekstra, H. van Tinteren and R. Boellaard, "Repeatability of Metabolically Active Volume Measurements with ^{18}F -FDG and ^{18}F -FLT PET in Non-Small Cell Lung Cancer," *Journal of Nuclear Medicine*, Vol. 51, No. 12, 2010, pp. 1870-1877. [doi:10.2967/jnumed.110.077255](https://doi.org/10.2967/jnumed.110.077255)
- [3] P. Vera, P. Bohn, A. Edet-Sanson, A. Salles, S. Hapdey, I. Gardin, J. F. Ménard, R. Modzelewski, L. Thiberville and B. Dubray, "Simultaneous Positron Emission Tomography (PET) Assessment of Metabolism with ^{18}F -Fluoro-2-Deoxy-D-Glucose (FDG), Proliferation with ^{18}F -Fluoro-Thymidine (FLT), and Hypoxia with ^{18}F -Fluoro-Misonidazole (F-Miso) before and during Radiotherapy in Patients with Non-Small-Cell Lung Cancer (NSCLC): A Pilot Study," *Radiotherapy and Oncology*, Vol. 98, No. 1, 2011, pp. 109-116. [doi:10.1016/j.radonc.2010.10.011](https://doi.org/10.1016/j.radonc.2010.10.011)
- [4] W. Yang, Y. Zhang, Z. Fu, J. Yu, X. Sun, D. Mu and A. Han, "Imaging of Proliferation with ^{18}F -FLT PET/CT Versus ^{18}F -FDG PET/CT in Non-Small-Cell Lung Cancer," *European Journal of Nuclear Medicine and Molecular*, Vol. 37, No. 7, 2010, pp. 1291-1299. [doi:10.1007/s00259-010-1412-6](https://doi.org/10.1007/s00259-010-1412-6)
- [5] Y. Yamamoto, Y. Nishiyama, S. Ishikawa, J. Nakano, S. S. Chang, S. Bandoh, N. Kanaji, R. Haba, Y. Kushida and M. Ohkawa, "Correlation of ^{18}F -FLT and ^{18}F -FDG Uptake on PET with Ki-67 Immunohistochemistry in Non-Small Cell Lung Cancer," *European Journal of Nuclear Medicine and Molecular*, Vol. 34, No. 10, 2007, pp. 1610-1616. [doi:10.1007/s00259-007-0449-7](https://doi.org/10.1007/s00259-007-0449-7)
- [6] S. A. Nehmeh, N. Y. Lee, H. Schröder, O. Squire, P. B. Zanzonico, Y. E. Erdi, C. Greco, G. Mageras, H. S. Pham, S. M. Larson, C. C. Ling and J. L. Humm, "Reproducibility of Intratumor Distribution of ^{18}F -Fluoromisonidazole in Head and Neck Cancer," *International Journal of Radiation Oncology, Biology, Physics*, Vol. 70, No. 1, 2008, pp. 235-242. [doi:10.1016/j.ijrobp.2007.08.036](https://doi.org/10.1016/j.ijrobp.2007.08.036)
- [7] A. K. Buck, G. Halter, H. Schirrmeister, J. Kotzerke, I. Wurziger, G. Glatting, T. Mattfeldt, B. Neumaier, S. N. Reske and M. Hetzel, "Imaging Proliferation in Lung Tumors with PET: ^{18}F -FLT versus ^{18}F -FDG," *Journal of Nuclear Medicine*, Vol. 44, No. 9, 2003, pp. 1426-1431.
- [8] X. F. Li, Y. Ma, X. Sun, J. L. Humm, C. C. Ling and J. A. O'Donoghue, "High ^{18}F -FDG Uptake in Microscopic Peritoneal Tumors Requires Physiologic Hypoxia," *Journal of Nuclear Medicine*, Vol. 51, No. 4, 2010, pp. 632-638. [doi:10.2967/jnumed.109.071233](https://doi.org/10.2967/jnumed.109.071233)
- [9] P. Burgman, J. A. O'Donoghue, J. L. Humm and C. C. Ling, "Hypoxia-Induced Increase in FDG Uptake in MCF7 Cells," *Journal of Nuclear Medicine*, Vol. 42, No. 1, 2001, pp. 170-175.
- [10] A. Pugachev, S. Ruan, S. Carlin, S. M. Larson, J. Campa, C. C. Ling and J. L. Humm, "Dependence of FDG Uptake on Tumor Microenvironment," *International Journal of Radiation Oncology, Biology, Physics*, Vol. 62, No. 2, 2005, pp. 545-553. [doi:10.1016/j.ijrobp.2005.02.009](https://doi.org/10.1016/j.ijrobp.2005.02.009)
- [11] T. Tanaka, T. Furukawa, S. Fujieda, S. Kasamatsu, Y. Yonekura and Y. Fujibayashi, "Double-Tracer Autoradiography with Cu-ATSM/FDG and Immunohistochemical Interpretation in Four Different Mouse Implanted Tumor Models," *Nuclear Medicine and Biology*, Vol. 33, No. 6, 2006, pp. 743-750. [doi:10.1016/j.nucmedbio.2006.05.005](https://doi.org/10.1016/j.nucmedbio.2006.05.005)
- [12] P. Zanzonico, J. Campa, D. Polycarpe-Holman, G. Forster, R. Finn, S. Larson, J. Humm and C. Ling, "Animal-Specific Positioning Molds for Registration of Repeat Imaging Studies: Comparative Micropet Imaging of ^{18}F -Labeled Fluoro-Deoxyglucose and Fluoro-Misonidazole in Rodent Tumors," *Nuclear Medicine and Biology*, Vol. 33, No. 1, 2006, pp. 65-70. [doi:10.1016/j.nucmedbio.2005.07.011](https://doi.org/10.1016/j.nucmedbio.2005.07.011)
- [13] C. S. Dence, D. E. Ponde, M. J. Welch and J. S. Lewis, "Autoradiographic and Small-Animal PET Comparisons between ^{18}F -FMISO, ^{18}F -FDG, ^{18}F -FLT and the Hypoxic Selective ^{64}Cu -ATSM in a Rodent Model of Cancer," *Nuclear Medicine and Biology*, Vol. 35, No. 6, 2008, pp. 713-720. [doi:10.1016/j.nucmedbio.2008.06.001](https://doi.org/10.1016/j.nucmedbio.2008.06.001)
- [14] E. G. Troost, P. Laverman, M. E. Philippens, J. Lok, A. J. van der Kogel, W. J. Oyen, O. C. Boerman, J. H. Kaanders and J. Bussink, "Correlation of [^{18}F]FMISO Autoradiography and Pimonidazole Immunohistochemistry in Human Head and Neck Carcinoma Xenografts," *European Journal of Nuclear Medicine and Molecular*, Vol. 35, No. 10, 2008, pp. 1803-1811. [doi:10.1007/s00259-008-0772-7](https://doi.org/10.1007/s00259-008-0772-7)
- [15] R. H. Thomlinson and L. H. Gray, "The Histological Structure of Some Human Lung Cancers and the Possible Implications for Radiotherapy," *British Journal of Cancer*, Vol. 9, No. 4, 1955, pp. 539-549. [doi:10.1038/bjc.1955.55](https://doi.org/10.1038/bjc.1955.55)
- [16] E. E. Graves, A. Maity and Q. T. Le, "the Tumor Microenvironment in Non-Small Cell Lung Cancer," *Seminars in Radiation Oncology*, Vol. 20, No. 3, 2010, pp. 156-163. [doi:10.1016/j.semradonc.2010.01.003](https://doi.org/10.1016/j.semradonc.2010.01.003)
- [17] D. Hanahan and R. A. Weinberg, "Hallmarks of Cancer: The Next Generation," *Cell*, Vol. 144, No. 5, 2011, pp. 646-674.
- [18] T. Huang, A. C. Civelek, J. Li, H. Jiang, C. K. Ng, G. C. Postel, B. Shen and X. F. Li, "Tumor Microenvironment-Dependent ^{18}F -FDG, ^{18}F -Fluorothymidine, and ^{18}F -Misonidazole Uptake: A Pilot Study in Mouse Models of Human Non-Small Cell Lung Cancer," *Journal of Nuclear Medicine*, Vol. 53, No. 8, 2012, pp. 1262-1268. [doi:10.2967/jnumed.111.098087](https://doi.org/10.2967/jnumed.111.098087)
- [19] X. F. Li, S. Carlin, M. Urano, J. Russell, C. C. Ling and J. A. O'Donoghue, "Visualization of Hypoxia in Microscopic Tumors by Immunofluorescent Microscopy," *Cancer Research*, Vol. 67, No. 16, 2007, pp. 7646-7653. [doi:10.1158/0008-5472.CAN-06-4353](https://doi.org/10.1158/0008-5472.CAN-06-4353)
- [20] A. S. Kennedy, J. A. Raleigh, G. M. Perez, D. P. Calkins, D. E. Thrall, D. B. Novotny and M. A. Varia, "Proliferation and Hypoxia in Human Squamous Cell Carcinoma of the Cervix: First Report of Combined Immunohistochemical Assays," *International Journal of Radiation Oncology, Biology, Physics*, Vol. 37, No. 4, 1997,

- pp. 897-905. doi:10.1016/S0360-3016(96)00539-1
- [21] R. E. Durand and J. A. Raleigh, "Identification of Non-proliferating but Viable Hypoxic Tumor Cells *in Vivo*," *Cancer Research*, Vol. 58, No. 16, 1998, pp. 3547-3550.
- [22] X. F. Li, P. Zanzonico, C. C. Ling and J. O'Donoghue, "Visualization of Experimental Lung and Bone Metastases in Live Nude Mice by X-Ray Micro-Computed Tomography," *Technology in Cancer Research and Treatment*, Vol. 5, No. 2, 2006, pp. 147-155.
- [23] M. D. Cameron, E. E. Schmidt, N. Kerkvliet, K. V. Nadkarni, V. L. Morris, A. C. Groom, A. F. Chambers and I. C. MacDonald, "Temporal Progression of Metastasis in Lung: Cell Survival, Dormancy, and Location Dependence of Metastatic Inefficiency," *Cancer Research*, Vol. 60, No. 9, 2000, pp. 2541-2546.
- [24] Y. Maniwa, M. Okada, N. Ishii and K. Kiyooka, "Vascular Endothelial Growth Factor Increased by Pulmonary Surgery Accelerates the Growth of Micrometastases in Metastatic Lung Cancer," *Chest*, Vol. 114, No. 6, 1998, pp. 1668-1675. doi:10.1378/chest.114.6.1668
- [25] T. Hiraga, S. Kizaka-Kondoh, K. Hirota, M. Hiraoka and T. Yoneda, "Hypoxia and Hypoxia-Inducible Factor-1 Expression Enhance Osteolytic Bone Metastases of Breast Cancer," *Cancer Research*, Vol. 67, No. 9, 2007, pp. 4157-4563. doi:10.1158/0008-5472.CAN-06-2355
- [26] X. F. Li, S. Kinuya, K. Yokoyama, K. Koshida, H. Mori, K. Shiba, N. Watanabe, N. Shuke, T. Michigishi and N. Tonami, "Benefits of Combined Radioimmunotherapy and Anti-Angiogenic Therapy in a Liver Metastasis Model of Human Colon Cancer Cells," *European Journal of Nuclear Medicine and Molecular*, Vol. 29, No. 12, 2002, pp. 1669-1674. doi:10.1007/s00259-002-0997-9
- [27] X. F. Li, X. Sun, Y. Ma, M. Suehiro, M. Zhang, J. Russell, J. L. Humm, C. C. Ling and J. A. O'Donoghue, "Detection of Hypoxia in Microscopic Tumors Using ¹³¹I-Labeled Iodo-Azomycin Galactopyranoside (¹³¹I-IAZGP) Digital Autoradiography," *European Journal of Nuclear Medicine and Molecular*, Vol. 37, No. 2, 2010, pp. 339-348. doi:10.1007/s00259-009-1310-y
- [28] X. F. Li and J. A. O'Donoghue, "Hypoxia in Microscopic Tumors," *Cancer Letters*, Vol. 264, No. 2, 2008, pp. 172-180. doi:10.1016/j.canlet.2008.02.037
- [29] A. S. Ljungkvist, J. Bussink, J. H. Kaanders, P. F. Rijken, A. C. Begg, J. A. Raleigh and A. J. van der Kogel, "Hypoxic Cell Turnover in Different Solid Tumor Lines," *International Journal of Radiation Oncology, Biology, Physics*, Vol. 62, No. 4, 2005, pp. 1157-168. doi:10.1016/j.ijrobp.2005.03.049
- [30] J. A. Raleigh, S. C. Chou, G. E. Arteel and M. R. Horsman, "Comparisons among Pimonidazole Binding, Oxygen Electrode Measurements, and Radiation Response in C3H Mouse Tumors," *Radiation Research*, Vol. 151, No. 5, 1999, pp. 580-589. doi:10.2307/3580034
- [31] J. H. Kaanders, K. I. Wijffels, H. A. Marres, A. S. Ljungkvist, L. A. Pop, F. J. van den Hoogen, P. C. de Wilde, J. Bussink, J. A. Raleigh and A. J. van der Kogel, "Pimonidazole Binding and Tumor Vascularity Predict for Treatment Outcome in Head and Neck Cancer," *Cancer Research*, Vol. 62, No. 23, 2002, pp. 7066-7074.
- [32] J. A. Raleigh, D. P. Calkins-Adams, L. H. Rinker, C. A. Ballenger, M. C. Weissler, W. C. Fowler Jr., D. B. Novotny and M. A. Varia, "Hypoxia and Vascular Endothelial Growth Factor Expression in Human Squamous Cell Carcinomas Using Pimonidazole as a Hypoxia Marker," *Cancer Research*, Vol. 58, No. 17, 1998, pp. 3765-3768.
- [33] A. S. Ljungkvist, J. Bussink, P. F. Rijken, J. A. Raleigh, J. Denekamp and A. J. Van Der Kogel, "Changes in Tumor Hypoxia Measured with a Double Hypoxic Marker Technique," *International Journal of Radiation Oncology, Biology, Physics*, Vol. 48, No. 5, 2000, pp. 1529-1538. doi:10.1016/S0360-3016(00)00787-2
- [34] J. A. O'Donoghue, P. Zanzonico, A. Pugachev, B. Wen, P. Smith-Jones, S. Cai, E. Burnazi, R. D. Finn, P. Burgman, S. Ruan, J. S. Lewis, M. J. Welch, C. C. Ling and J. L. Humm, "Assessment of Regional Tumor Hypoxia Using ¹⁸F-Fluoromisonidazole and ⁶⁴Cu(II)-Diacetyl-Bis (N4-Methylthiosemicarbazone) Positron Emission Tomography: Comparative Study Featuring Micropet Imaging, Po₂ Probe Measurement, Autoradiography, and Fluorescent Microscopy in the R3327-AT and FaDu Rat Tumor Models," *International Journal of Radiation Oncology, Biology, Physics*, Vol. 61, No. 5, 2005, pp. 1493-1502. doi:10.1016/j.ijrobp.2004.12.057
- [35] S. Ben-Haim and P. Ell, "¹⁸F-FDG PET and PET/CT in the Evaluation of Cancer Treatment Response," *Journal of Nuclear Medicine*, Vol. 50, No. 1, 2009, pp. 88-99. doi:10.2967/jnumed.108.054205
- [36] R. A. Dierckx and C. Van de Wiele, "FDG Uptake, a Surrogate of Tumour Hypoxia?" *European Journal of Nuclear Medicine and Molecular*, Vol. 35, No. 8, 2008, pp. 1544-1549. doi:10.1007/s00259-008-0758-5
- [37] G. L. Semenza, "Targeting HIF-1 for Cancer Therapy," *Nature Reviews Cancer*, Vol. 3, No. 10, 2003, pp. 721-732. doi:10.1038/nrc1187
- [38] L. Bentzen, S. Keiding, M. R. Horsman, L. Falborg, S. B. Hansen and J. Overgaard, "Feasibility of Detecting Hypoxia in Experimental Mouse Tumours with ¹⁸F-Fluorinated Tracers and Positron Emission Tomography—A Study Evaluating [¹⁸F]Fluoro-2-Deoxy-D-Glucose," *Acta Oncologica*, Vol. 39, No. 35, 2000, pp. 629-637. doi:10.1080/028418600750013320
- [39] L. Dubois, W. Landuyt, K. Haustermans, P. Dupont, G. Bormans, P. Vermaelen, E. Verbeken and L. Mortelmans, "Evaluation of Hypoxia in an Experimental Rat Tumour Model by [¹⁸F]Fluoromisonidazole PET and Immunohistochemistry," *British Journal of Cancer*, Vol. 91, No. 11, 2004, pp. 1947-1954. doi:10.1038/sj.bjc.6602219
- [40] F. He, X. Deng, B. Wen, Y. Liu, X. Sun, L. Xing, A. Minami, Y. Huang, Q. Chen, P. B. Zanzonico, C. C. Ling and G. C. Li, "Noninvasive Molecular Imaging of Hypoxia in Human Xenografts: Comparing Hypoxia-Induced Gene Expression with Endogenous and Exogenous Hypoxia Markers," *Cancer Research*, Vol. 68, No. 20, 2008, pp. 8597-8606. doi:10.1158/0008-5472.CAN-08-0677
- [41] R. V. Iyer, E. L. Engelhardt, C. C. Stobbe, R. F. Schneider and J. D. Chapman, "Preclinical Assessment of Hypoxic Marker Specificity and Sensitivity," *International Journal of Radiation Oncology, Biology, Physics*, Vol. 42, No. 42, 1998, pp. 741-745.

- [doi:10.1016/S0360-3016\(98\)00315-0](https://doi.org/10.1016/S0360-3016(98)00315-0)
- [42] P. Zanzonico, J. O'Donoghue, J. D. Chapman, R. Schneider, S. Cai, S. Larson, B. Wen, Y. Chen, R. Finn, S. Ruan, L. Gerweck, J. Humm and C. Ling, "Iodine-124-Labeled Iodo-Azomycin-Galactoside Imaging of Tumor Hypoxia in Mice with Serial Micropet Scanning," *European Journal of Nuclear Medicine and Molecular*, Vol. 31, No. 1, 2004, pp. 117-128. [doi:10.1007/s00259-003-1322-y](https://doi.org/10.1007/s00259-003-1322-y)
- [43] C. C. Riedl, P. Brader, P. B. Zanzonico, Y. S. Chun, Y. Woo, P. Singh, S. Carlin, B. Wen, C. C. Ling, H. Hricak and Y. Fong, "Imaging Hypoxia in Orthotopic Rat Liver Tumors with Iodine 124-Labeled Iodoazomycin Galactopyranoside PET," *Radiology*, Vol. 248, No. 2, 2008, pp. 561-570. [doi:10.1148/radiol.2482071421](https://doi.org/10.1148/radiol.2482071421)
- [44] K. Wang, E. Yorke, S. A. Nehmeh, J. L. Humm and C. C. Ling, "Modeling Acute and Chronic Hypoxia Using Serial Images of ^{18}F -FMISO PET," *Medical Physics*, Vol. 36, No. 10, 2009, pp. 4400-4408. [doi:10.1118/1.3213092](https://doi.org/10.1118/1.3213092)